International Journal of Theoretical & Applied Sciences, **17**(2): 124-129(2025)

ISSN No. (Print): 0975-1718
ISSN No. (Online): 2249-3247

DFT Study of Type-II $SnBr_2$/CuI vdW Heterostructure: Implications for Thermophotovoltaic Devices

P. H. Jariwala[1,*], Yashasvi Naik[2], P. R. Parmar[2] and H. R. Mahida[2]
[1]Department of Physics, Navyug Science College, Surat (Gujarat), India.
[2]Department of Physics, Veer Narmad South Gujarat University, Surat (Gujarat), India.

(Corresponding author: P. H. Jariwala)*
(Received 27 August, 2025; Accepted 29 September, 2025, Published: 09 October, 2025)
(Published by Research Trend, Website: www.researchtrend.net)

ABSTRACT: In present investigation, first-principle investigation on the structural stability and tunable optoelectronic characteristics of a $SnBr_2$/CuI van der Waals heterostructure (vdW HTS). The stability of the vdW HTS is also verified by adhesion energy calculations and ab initio molecular dynamics (AIMD) simulations, exhibiting its energetic and thermal stability. Electronic band structure calculations determine $SnBr_2$/CuI vdW HTS to exhibit a direct bandgap near 1.17 eV within the HSE06 functional, in the optimum bandgap regime for solar absorbers. Crucially, the type-II band alignment enables spatial separation of photogenerated holes and electrons, thus inhibiting recombination and favoring carrier transportation across the interface. Charge density difference analysis also validates interfacial charge reconstructions in accordance with efficient carrier exchange. The optical calculations indicate a clear red-shifted absorption edge into the visible regime, along with an increased absorption coefficient over the pure monolayer counterparts, implying enhanced light-harvesting capability. Together, these findings establish the $SnBr_2$/CuI vdW HTS to offer excellent structural stability alongside tunable optoelectronic performance, thus making it an extremely promising next-generation solar and nano-optoelectronic contender.

Keywords: vdW Heterostructure, Thermophotovoltaic, DFT, Type-II semiconductor.

INTRODUCTION

To achieve efficient carrier separation in photoelectric, photovoltaic devices, it is crucial to explore suitable materials and structures. One promising solution is the use of van der Waals heterostructure (vdw HTS) with a type-II band alignment. These HTSs consist of two-different monolayers (MLs) stacked on top of each other without forming chemical bonds in between. The concept of vdw HTS was first introduced by Geim *et al.* 2013, and it has gained significant attention in the field of materials research (Meng *et al*., 2021). The weak vdw forces between these monolayers allow them to retain their original monolayer's optoelectronic characteristics, while the interlayer interaction brings out the novel characteristics. Many researchers have successfully constructed various 2D vdw HTS such as PtS_2/ZrS_2 (Parmar *et al*., 2023), $GaTe/ZnI_2$, $PtSe_2$/GaSe (Parmar *et al*., 2023), and many others. The discovery of graphene (Novoselov *et al*., 2005) has brought new insight into 2D materials. After that, many 2D materials are studied extensively because of their novel properties and potential applications (Khengar *et al*., 2022, Modi *et al*., 2023). Of all these various 2D materials, halides-dihalides have gained research interest due to their interesting properties, potential applications, and tunable bandgap (Hu *et al*., 2020). Recently, $SnBr_2$ has been theoretically investigated, having an indirect bandgap of 3.02 eV (Naik *et al*., 2023). While CuI has a direct bandgap having an application in photovoltaic devices (Amrani *et al*., 2006). Due to these excellent properties of $SnBr_2$ and CuI MLs, we choose to construct $SnBr_2$/CuI vdw HTS. Recently, 2D materials are explored for many novel applications such as Gas sensors (Peng *et al*., 2021), storage devices (Mortazavi *et al*., 2016), Thermophotovoltaic (TPV) devices (Ismail *et al*., 2024), photocatalysis (Shakil *et al*., 2023), etc. Among which, TPV is gaining more research interest due its various potential use. TPV devices are energy conversion systems that directly transform thermal radiation into electricity which is the same fundamental principle as photovoltaic cells. Such TPV devices not only use sunlight just like solar cell but it harnesses the thermal radiation emitted from high-temperature sources such as combustion systems, concentrated solar absorbers, nuclear reactors, or even industrial waste heat. A typical TPV system consists of a thermal emitter, which radiates a broad spectrum of photons when heated to elevated temperatures, and a photovoltaic cell that absorbs these photons to generate electron–hole pairs and produce electrical power (Agarwal and Prajapati 2018). Spectral control elements such as filters or photonic structures are used in TPV which reflects sub-bandgap photons back to the emitter and hence efficiency improved.

The efficiency of TPV devices strongly depends on the choice of semiconductor material for the photovoltaic cell, as the bandgap must be carefully matched with the spectral distribution of the thermal emitter (Ahmed *et al.*, 2025). Low bandgap semiconductors in the range of 0.2–0.7 eV, including materials such as InGaAsP (Tuley and Nicholas 2010), GeTe (Abir *et al*., 2023), have been

widely studied because of their ability to absorb near-infrared thermal radiation effectively. In addition, achieving direct bandgaps and favorable carrier dynamics through Type-II band alignment in heterostructures has been shown to improve photon absorption and charge extraction, both of which are essential for efficient device performance (Almayyali *et al*., 2023). In this context, recent advances in two-dimensional (2D) materials and van der Waals heterostructures have opened new possibilities for TPV device design, owing to their tunable band structures, strong light–matter interactions, and potential to achieve Type-II band alignment with direct bandgaps. These features make them promising candidates for next-generation TPV applications.

Currently, no systematic research has been found on the $SnBr_2$/CuI vdW Heterostructure for the implications in Thermophotovoltaic Devices. So, this research consists of the DFT investigation on $SnBr_2$/CuI vdw HTS thermophotovoltaic Devices.

COMPUTATIONAL DETAILS

In this research, all the simulations have been performed within the DFT framework (Orio *et al*., 2009) by Quantum Espresso software. The exchange-correlation functional of the electron is described by utilizing the Generalized Gradient Approximation (GGA) given by the Perdew-Burke-Eruzerhof (PBE) (Perdew *et al*., 1996). To obtain a more accurate bandgap, a hybrid functional HSE06 given by Heyd-Scuseria-Ernzerhof (Heyd *et al*., 2003) is utilized. The DFT-D3 (Grimme *et al*., 2011) method given by Grimme has been utilized to represent the vdw interactions. A thick vacuum of 25 Å is given in a perpendicular direction in order to prevent interactions between two layers. The energy and force threshold is set to 10^{-8} Ry and 10^{-4} Ry/Bohr, respectively, to obtain structural optimization and system convergence. The Monkhorst-Pack k-point grid is fixed at 6×6×1 and plane wave energy cut-off is fixed at 550 Ry. The optical properties are obtained by using the Norm-conserving pseudopotential and frequency-dependent complex dielectric function ε (ω).

RESULTS AND DISCUSSIONS

A. Structural Properties

The monolayers $SnBr_2$ and CuI have similar hexagonal symmetry and almost the same lattice parameter, so it feasible to construct heterostructure easily. The obtained lattice constant (a) of $SnBr_2$/CuI vdw HTS, $SnBr_2$ ML, and CuI ML are 4.32 Å, 4.37 Å, and 4.33 Å, respectively. The lattice mismatch between their constitute monolayer for $SnBr_2$/CuI vdw HTS is given by equation $\delta = \frac{a_{CuI} - a_{SnBr_2}}{a_{CuI}}$ (Parmar *et al*., 2023), which is 1.14% for this vdw HTS. The optimized structure of constructed $SnBr_2$/CuI vdw HTS is illustrated in Fig. 1(a).

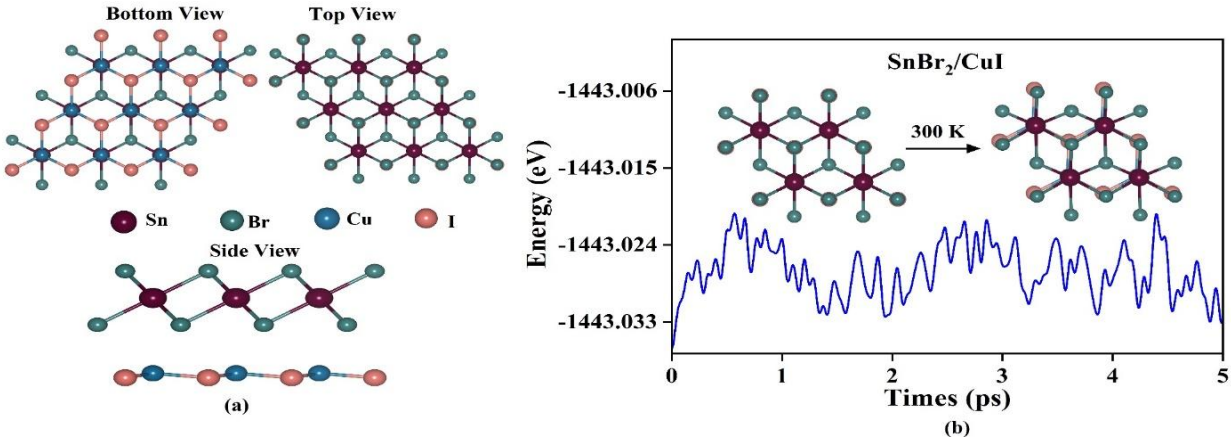

Fig. 1. (a) Optimized structure and (b) AIMD calculation of $SnBr_2$/CuI vdw HTS.

To check the energetic stability of this constructed vdw HTS, we have to find its adhesion energy E_{ae} that is given by equation (Parmar *et al*., 2022), $E_{ae} = E_{vdw\ HTS} - E_{SnBr_2} - E_{CuI}$. Where $E_{vdw\ HTS}$ is the total energy of a HTS, and E_{SnBr2} and E_{CuI} represent the energy of their respective monolayers. The obtained negative value of adhesion energy -1.01 eV for the $SnBr_2$/CuI vdw HTS shows that the material is energetically stable. However, the AIMD simulation is also performed to ensure the thermal stability of $SnBr_2$/CuI vdw HTS for 5 ps with a time interval of 1fs. The obtained results as shown in Fig. 1(b), illustrates that there is minimal deviation in total energy and negligible structural fluctuations throughout the entire simulation. Hence, the constructed $SnBr_2$/CuI vdw HTS is energetically and thermally stable material.

It can also be added that the extremely low lattice mismatch (1.14%) implies negligible interfacial strain, favorable for the retention of the intrinsic quality of the constituting layers while allowing for tight interlayer coupling (Guo *et al*., 2017). The geometrically optimized structure implies that the van der Waals interaction maintains the interlayer separation without structural distortions, confirming structural soundness. Such low values for the mismatch also favour easier experimental realization, due to the lack of strain-related defects. Furthermore, the stability also agreed by the room-temperature AIMD implies the potential for the heterostructure to survive real-device operation conditions. Collectively, these results imply that the $SnBr_2$/CuI vdW HTS possesses the dual characteristic of robustness and compatibility, preconditions for the

realization of practical optoelectronic as well as photovoltaic device fabrication.

B. Electronic Properties

Since $SnBr_2$ ML, CuI ML, and $SnBr_2$/CuI vdw HTS have hexagonal symmetry, the band diagram is obtained along highly symmetric direction 'Γ-M-K-Γ' with HSE06 functional as shown in Fig. 2(a,b,c). The $SnBr_2$ ML has an indirect bandgap of 3.02 eV, while CuI ML has a direct bandgap of 2.50 eV. Interestingly, $SnBr_2$/CuI vdw HTS exhibits a direct bandgap of 1.21 eV, which is lesser than each monolayer of constructive components. The CBM resembles $SnBr_2$ while VBM mainly originates from CuI. Hence, in the presence of radiation, the $SnBr_2$/CuI vdw HTS exhibits efficient electron transfer, resulting in the effective separation of photoexcited electron-hole pairs. These findings also highlight the enhanced optical properties. The Fig. 2(d) displays the Projected Density of State (PDOS).

It is seen that Cu-d state is more dominant in valance band while Br-p and Sn-p states have significant effect in conduction band. Additionally, the overlap of Cu-d states with Sn-p/Br-p states around the Fermi level indicates interlayer hybridization, which enhances interfacial coupling and supports efficient charge transfer. The band curvature in Fig. 2 also suggests relatively light effective masses for electrons in the $SnBr_2$ conduction band and holes in the CuI valence band. Lower effective masses are typically associated with higher carrier mobilities, which is a desirable feature for fast charge transport in photovoltaic applications. The materials work function Φ is characteristics as the energy required to eliminate an electron from its surface is obtained by employing the equation, $\Phi = E_{vac} - E_f$, where E_f and E_{vac} denote the fermi and vacuum level. The obtained Φ is 8.71 eV for vdw HTS.

As shown in Fig. 3(a), the CuI ML exhibits a higher work function compared to the $SnBr_2$ ML, which indicates that upon contact electrons will transfer from CuI to $SnBr_2$ surface until their fermi level matches. Furthermore, the charge density difference Δρ is obtained (Parmar *et al*., 2023) from $\Delta\rho = \Delta\rho_{vdw\ HTS} - \Delta\rho_{SnBr_2} - \Delta\rho_{CuI}$. The yellow clouds below $SnBr_2$ ML indicate charge accumulation, while green spheres above CuI ML suggest charge depletion, implying substantial charge transfer from CuI ML to $SnBr_2$ ML, as depicted in Fig. 3(b). The redistribution of charges forms an intrinsic inbuilt electric field at the junction, which in turn drives the photogenerated carriers away and hinders the loss due to recombination. The generated dipole layer at the interface at the end adjusts the electrostatic potential at the junction, favoring enhanced type-II band alignment and easier carrier separation. Such effects demonstrate the working principle of a normal p–n junction but in the pure 2D vdW regime (Chapin *et al*., 1954).

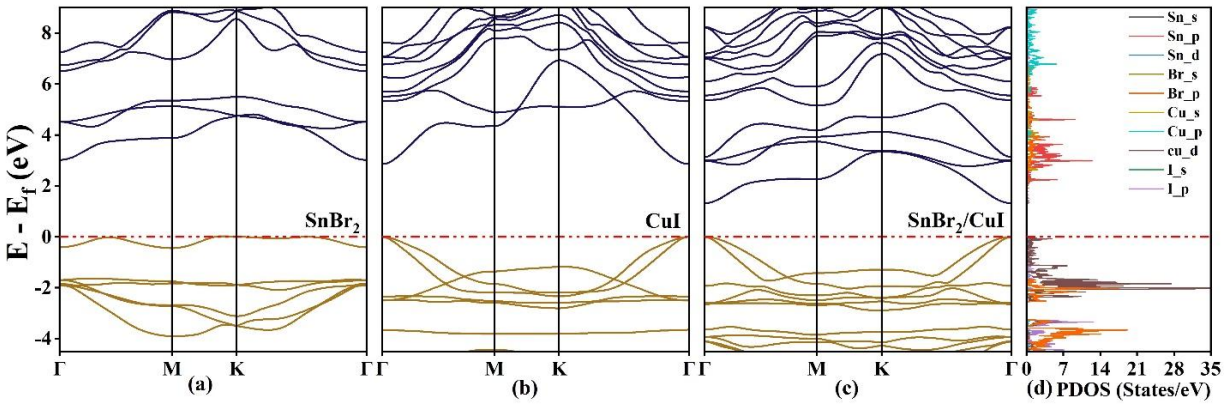

Fig. 2. Band structure of (a) SnBr2 ML (b) CuI ML (c) $SnBr_2$/CuI vdw HTS and (d) PDOS of $SnBr_2$/CuI vdw HTS.

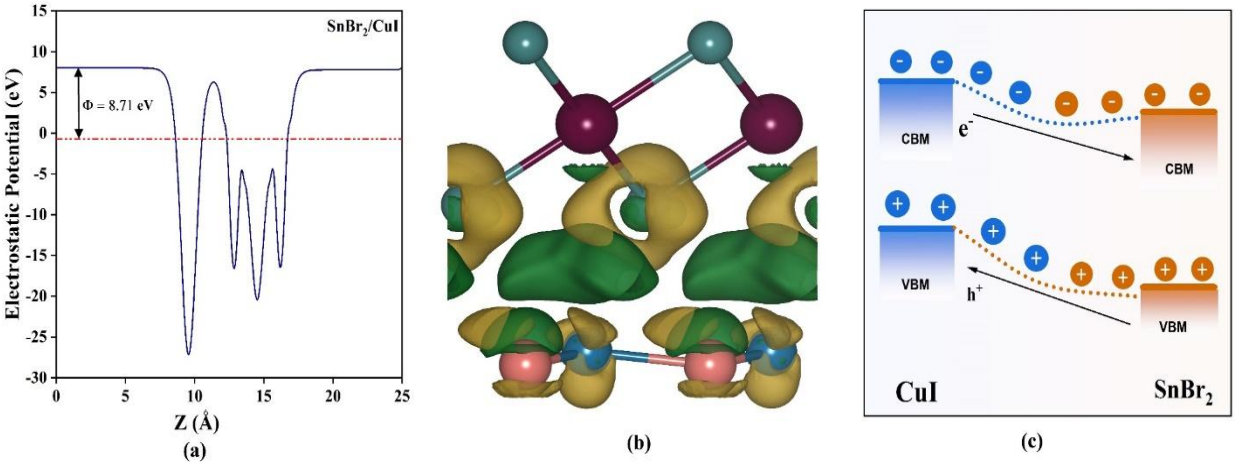

Fig. 3. (a) Work Function (b) Charge density (c) Charge transfer with band alignment.

Besides the photovoltaic uses, the offset alignment can be utilized for photocatalytic reaction, where spatially separated carrier pairs are utilized to drive reduction and oxidation processes on different layers (Dalsaniya *et al.*, 2021).

The band alignment is displayed in Fig. 3(c). Under solar light, the $SnBr_2$/CuI vdw HTS exhibits photogenerated electron transfer from CuI ML to the $SnBr_2$ conduction band and photoexcited holes move to CuI valance band, achieving spatial electron-hole separation. This is attributed to the type-II band alignment, effectively reducing electron-hole recombination.

C. Optical Properties

The optical response is calculated from the dielectric function (that is the function of frequency) ε(ω) given as $\varepsilon(\omega) = \varepsilon^1(\omega) + i\varepsilon^2(\omega)$. Here, $\varepsilon^1(\omega)$ and $\varepsilon^2(\omega)$ corresponds to the real and imaginary portion, respectively. The real part in Fig. 4(a) shows that the static dielectric constant (SDC) of $SnBr_2$ ML, CuI ML, and $SnBr_2$/CuI vdw HTS is 2.54, 1.76, 2.91, respectively. The increment in SDC of $\varepsilon^1(\omega)$ implies that lower exciton binding energy which leads to an effective hole and electrons separation. The presence of a negative value indicates the metallic characteristics at that particular frequency. The dielectric function's imaginary portion is related to the interband transition, which is shown in Fig. 4(b) exhibits several distinct peaks. Further, the relation between absorption coefficient and energy is displayed in Fig. 4(c). and is obtained the equation (Mehta *et al*., 2023),

$$\alpha(\omega) = \left(\frac{\sqrt{2}\omega}{c}\right)\left[(\varepsilon^1(\omega)^2 + \varepsilon^2(\omega)^2)^{\frac{1}{2}} - \varepsilon^1(\omega)\right]^{\frac{1}{2}}.$$

The highest peak is observed at 6.74 eV, 5.54 eV, and 7.55 eV for $SnBr_2$ ML, CuI ML, and $SnBr_2$/CuI vdw HTS, respectively. It is seen from the figure that the absorption of $SnBr_2$/CuI vdw HTS is enhanced from CuI ML. Also, $SnBr_2$/CuI vdw HTS exhibits a starting noticeable absorption in visible region in comparison with $SnBr_2$ ML. So, by comparing the absorption curve of both MLs with $SnBr_2$/CuI vdw HTS, it is seen that $SnBr_2$/CuI vdw HTS has better absorption performance. So, $SnBr_2$/CuI vdw HTS has great potential for efficient optoelectronic-nanoelectronics devices and photovoltaic application.

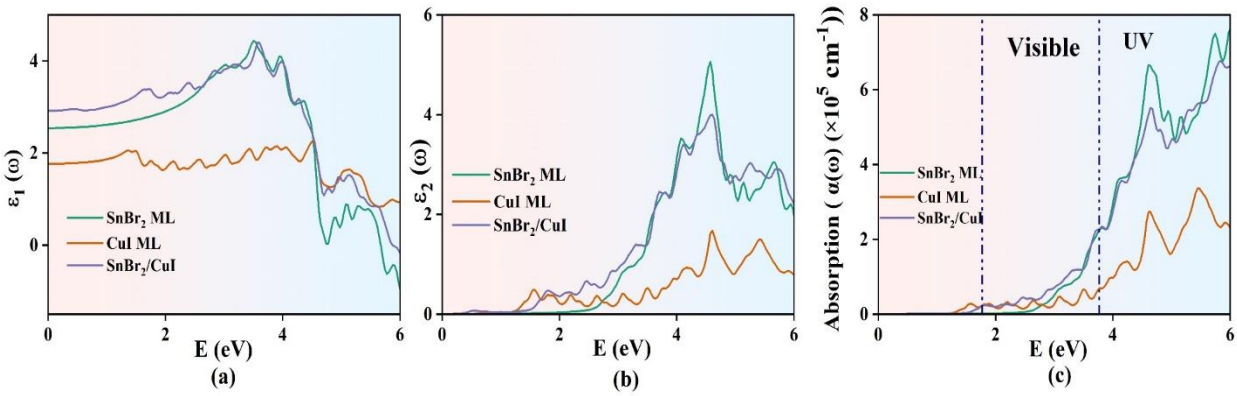

Fig. 4. (a) Real portion (b) Imaginary portion and (c) Absorption coefficient.

Besides the improved absorption, the red-shifted absorption edge for $SnBr_2$/CuI vdW HTS holds special significance, for it enables the material to exploit a larger fraction of the solar spectrum than either of the individual layers. The relatively larger dielectric constant also translates to lower exciton binding energy, implying that the excitons can be readily split into free carriers—a characteristic important for photovoltaic conversion. Lastly, the sharp absorption peaks in the UV regime point to possible suitability for UV photodetectors (Patel *et al*., 2021). The simultaneous occurrence of visible-range absorption and UV sensitivity also serves to reinforce the optoelectronic tunability of the heterostructure, making it suitable for various optoelectronic applications (Yang *et al*., 2019). Such spectral tunability is characteristic for vdW heterostructures and fortifies the candidacy for multifunctional devices for $SnBr_2$/CuI.

CONCLUSIONS

In this work, we have systematically investigated the structural and optoelectronic properties of the $SnBr_2$/CuI van der Waals heterostructure (vdW HTS) using first-principles density functional theory calculations. Our results confirm that the heterostructure is both energetically and thermally stable, as evidenced by the negative adhesion energy and the minimal fluctuations observed in AIMD simulations. The compatibility of lattice constants between $SnBr_2$ and CuI enables the formation of a stable interface with minimal mismatch, further supporting its structural integrity.

From an electronic point of view, $SnBr_2$/CuI vdW HTS has a direct bandgap in the region of about 1.17 eV, within the optimum value for photovoltaic absorbers. Note well that the type-II band alignment for efficient charge transfer over the interface takes place due to the spatial separation of electrons and holes in multiple layers. The band alignment strongly suppresses the recombination losses, thus increasing the probable efficiency in devices by virtue of this heterostructure. Charge density difference calculations and work functions are additional proof to confirm the taking place of the interfacial charge redistribution in support of effective carrier separation.

Optical characterizations reveal weak absorption in the visible regime for the pure $SnBr_2$ monolayer, while the $SnBr_2$/CuI heterostructure red-shifts the absorption edge to align the absorption within the visible regime. The above-mentioned features along with the relatively low value of the exciton binding energy indicated by the

larger dielectric constant direct towards efficient separation and generation of the photoexcited carrier pairs in the heterostructure. Consequently, the synergistic combination of inherent structural stability, appropriate band alignment, and improved optical response makes the $SnBr_2$/CuI vdW HTS an extremely viable prospect for next-generation photovoltaic and nano-optoelectronic devices. The $SnBr_2$/CuI vdW heterostructure demonstrates type-II band alignment and a direct bandgap, both of which are highly favorable for efficient carrier separation and strong light absorption. These features suggest that the system could be a promising candidate for thermophotovoltaic applications, where optimized bandgaps and charge dynamics are essential for high conversion efficiency.

FUTURE SCOPE

The SnBr2/CuI heterostructure from the present study has the appropriate stability, band alignment, and optical response for next-generation photovoltaic and TPV devices. Further simulations at the device level, experimental synthesis, and tuning by strain, doping, or external fields are suggested to further optimize the performance of SnBr2/CuI. Its strong interlayer charge separation and visible-range absorption also make it a good candidate for broader optoelectronic applications.

Acknowledgements. P. H. Jariwala sincerely thank the financial assistance provided in the form of minor research grants by Veer Narmad South Gujarat University, Grant No. UGC/17104/2023. The assistance proved helpful in obtaining computational infrastructure and analysis support in the current work on $SnBr_2$/CuI van der Waals heterostructures.

Conflict of Interest. The authors declare that they have no known financial or personal relationships that could have influenced the work reported in this paper. No competing interests exist.

REFERENCES

Abir, A. T., Mondal, B. K. and Hossain, J. (2023). Exploring the potential of GeTe for thermophotovoltaic cell applications. *Physica Scripta*, *98*, 125940.

Agarwal, S. and Prajapati, Y. K. (2018). Design of broadband absorber using 2D materials for thermophotovoltaic cell application. *Optics Communications*, *413*, 39–43.

Ahmed, S., Majid, A., Nasir, M., Islam, G. U., Ullah, S. A., Maqbool, N. *et al*. (2025). First-principles investigations of the physical properties of $CsSnI_3$ halide perovskite for thermophotovoltaic devices. *Journal of Inorganic and Organometallic Polymers and Materials*, (Online).

Almayyali, A. O. M., Jappor, H. R. and Muhsen, H. O. (2023). High hydrogen production in two-dimensional GaTe/ZnI_2 type-II heterostructure for water splitting. *Journal of Physics and Chemistry of Solids*, *178*, 111317.

Amrani, B., Benmessabih, T., Tahiri, M., Chiboub, I., Hiadsi, S. and Hamdache, F. (2006). Structural, elastic, electronic and optical properties of CuCl, CuBr and CuI under hydrostatic pressure: A first-principles study. *Physica B: Condensed Matter*, *381*, 179–186.

Chapin, D. M., Fuller, C. S. and Pearson, G. L. (1954). A new silicon p-n junction photocell for converting solar radiation into electrical power. *Journal of Applied Physics*, *25*, 676–677.

Dalsaniya, M. H., Gajaria, T. K., Som, N. N., Jha, P. K., Špiewak, P. and Kurzydłowski, K. J. (2021). Type-II GeAs/GaSe heterostructure as a suitable candidate for solar power conversion efficiency. *Solar Energy*, *223*, 87–99.

Geim, A. K., & Grigorieva, I. V. (2013). Van der Waals heterostructures. *Nature*, *499*(7459), 419-425.

Grimme, S., Antony, J., Ehrlich, S. and Krieg, H. (2011). A consistent and accurate ab initio parametrization of density functional dispersion correction (DFT-D) for the 94 elements H–Pu. *Journal of Chemical Physics*, *132*, 154104.

Guo, Z., Miao, N., Zhou, J., Sa, B. and Sun, Z. (2017). Strain-mediated type-I/type-II transition in MXene/blue phosphorene van der Waals heterostructures. *Journal of Materials Chemistry C*, *5*, 978–984.

Heyd, J., Scuseria, G. E. and Ernzerhof, M. (2003). Hybrid functionals based on a screened Coulomb potential. *Journal of Chemical Physics*, *118*, 8207–8215.

Hu, Y. F., Yang, J., Yuan, Y. Q. and Wang, J. W. (2020). GeI_2 monolayer: A model thermoelectric material from 300 to 600 K. *Philosophical Magazine*, *100*, 782–796.

Ismail, Md., Abir, A. T., Mondal, B. K., Chowdhury, M. A. H., Hossain, M., Rahaman, Md. M. and Hossain, J. (2024). Theoretical insights into narrow bandgap $CuFeS_2$ chalcopyrite for thermophotovoltaic applications. *Materials Today Communications*, *39*, 109089.

Khengar, S. J., Parmar, P. R. and Thakor, P. B. (2022). Strain-dependent structural and electronic properties of two-dimensional Janus In_2SeTe monolayer. *Materials Today: Proceedings*, *67*, 259–262.

Mehta, D., Modi, N., Khengar, S. J., Jariwala, P. H. and Thakor, P. B. (2023). $GaAlS_2$ Janus monolayer as a promising candidate for optoelectronic devices. *Materials Today: Proceedings*, 2–5.

Meng, L., Huang, Q., Liu, C., Li, H., Yan, W., Zhao, Q. and Yan, X. (2021). Robust type-II BP/AlN van der Waals heterostructure: A first-principles study. *Chemical Physics Letters*, *781*, 138989.

Modi, N., Naik, Y., Parmar, P. R., Jariwala, P. H., Shah, D. B. and Thakor, P. B. (2023). Strain engineering of Sc_2CBr_2 MXene monolayer by first-principle approach. *Materials Today: Proceedings*, (Online).

Mortazavi, B., Dianat, A., Rahaman, O., Cuniberti, G. and Rabczuk, T. (2016). Borophene as an anode material for Ca, Mg, Na or Li ion storage: A first-principles study. *Journal of Power Sources*, *329*, 456–461.

Naik, Y., Mehta, D., Parmar, P. R., Jariwala, P. H. and Thakor, P. B. (2023). Structural, electronic and optical properties of $SnBr_2$ monolayer by density functional approach. *Materials Today: Proceedings*, 1–4.

Novoselov, K. S., Jiang, D., Schedin, F., Booth, T. J., Khotkevich, V. V., Morozov, S. V. and Geim, A. K. (2005). Two-dimensional atomic crystals. *Proceedings of the National Academy of Sciences*, *102*(30), 10451–10453.

Orio, M., Pantazis, D. A. and Neese, F. (2009). Density functional theory. *Photosynthesis Research*, *102*, 443–453.

Parmar, P. R., Khengar, S. J. and Thakor, P. B. (2022). Structural and electronic properties of $PtSe_2$/GaP heterostructure. *Materials Today: Proceedings*, (Online).

Parmar, P. R., Khengar, S. J., Mehta, D., Sonvane, Y. and Thakor, P. B. (2023). Solar energy harvesting by a PtS_2/ZrS_2 van der Waals heterostructure. *New Journal of Chemistry*, (In press).

Parmar, P. R., Khengar, S. J., Sonvane, Y. K. and Thakor, P. B. (2023). Enhanced photocatalytic performance of stable type-II $PtSe_2$/GaSe van der Waals heterostructure. *Physical Chemistry Chemical Physics*, (Online).

Patel, V. R., Patel, A., Sonvane, Y. and Thakor, P. B. (2021). Optoelectronic properties of 2D heterojunction ZrO_2–MoS_2 material using first-principles calculations. *Solid State Communications*, 334–335, 114358.

Peng, R., Zhou, Q. and Zeng, W. (2021). First-principles study of Au-doped InN monolayer as adsorbent and gas sensing material for SF_6 decomposed species. *Nanomaterials*, *11*, 1708.

Perdew, J. P., Burke, K. and Ernzerhof, M. (1996). Generalized gradient approximation made simple. *Physical Review Letters*, *7s7*, 3865–3868.

Shakil, M., Shehzadi, I., Gillani, S. S. A., Al-Buriahi, M. S., Katubi, K. M. and Alrowaili, Z. A. (2023). GeSe/MoS_2 van der Waals heterostructure as a potential photocatalyst for water splitting: A DFT study. *Physica B: Condensed Matter*, *663*, 415008.

Tuley, R. S. and Nicholas, R. J. (2010). Band-gap dependent thermophotovoltaic device performance using InGaAs and InGaAsP. *Journal of Applied Physics*, *108*, 084516.

Yang, X., Singh, D., Xu, Z., Wang, Z. and Ahuja, R. (2019). Emerging Janus MoSeTe material for potential optoelectronic applications. *Journal of Materials Chemistry C*, *7*, 12312–12320.

How to cite this article: P. H. Jariwala, Yashasvi Naik, P. R. Parmar and H. R. Mahida (2025). DFT Study of Type-II $SnBr_2$/CuI vdW Heterostructure: Implications for Thermophotovoltaic Devices. *International Journal of Theoretical & Applied Sciences*, *17*(2): 124–129.